ACS OMEGA

Article

Cite This: ACS Omega 2019, 4, 13991−14003

http://pubs.acs.org/journal/acsodf

In Situ Immobilized Silver Nanoparticles on *Rubia tinctorum* Extract-Coated Ultrasmall Iron Oxide Nanoparticles: An Efficient Nanocatalyst with Magnetic Recyclability for Synthesis of Propargylamines by A^3 Coupling Reaction

Hojat Veisi,* Lida Mohammadi, Saba Hemmati, Taiebeh Tamoradi, and Pourya Mohammadi

Department of Chemistry, Payame Noor University, Tehran 19395-4697, Iran

ABSTRACT: This research suggests a green method for synthesizing hybrid magnetic nanocomposites that can be used as a reductant and a stabilizing agent for immobilizing metal nanoparticles (NPs). The central idea is the modification of magnetic NPs using *Rubia tinctorum* extract, which consists of numerous carbonyl and phenolic hydroxyl functional groups to increase adsorption of metals and chelate silver ions, and decrease the adsorption of silver ions by Ag NPs, in situ. Thus, the suggested catalyst preparation process does not require toxic reagents, additional reductants, and intricate instruments. To show the effectiveness of the plant extract in reducing and immobilizing Ag NPs, the structural, morphological, and physicochemical features of the particles are studied using Fourier-transform infrared spectroscopy, inductively coupled plasma atomic emission spectroscopy, field emission scanning electron microscopy, energy-dispersive X-ray spectroscopy, high-resolution transmission electron microscopy, vibrating sample magnetometry, X-ray diffraction analysis, and X-ray photoelectron spectroscopy. One of the advantages of the suggested method is to reduce the size of the magnetic NPs from 15−20 to 2−5 nm, in the presence of the extract. Additionally, the prepared Fe_3O_4@*R. tinctorum*/Ag nanocatalyst is demonstrated to exhibit a very high activity in the catalysis of the three-component reaction of aldehydes, amines, and alkynes (A^3 coupling) with good to high yields of diverse propargylamines. Moreover, the nanocatalyst can be recovered several times with no considerable leaching or loss of performance.

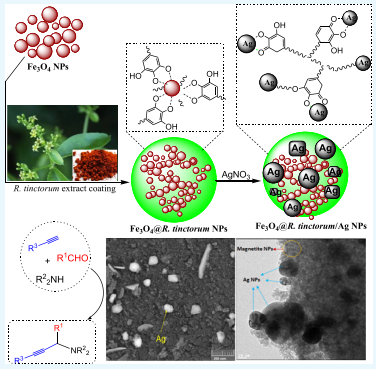

INTRODUCTION

Propargylamines (PPAs) play many main roles in the area of organic chemistry. They can be utilized as the precursors and building units of numerous nitrogen-containing heterocyclic compounds; meanwhile, they can also be used as the key intermediates in synthesizing bioactive medicines and natural products.[1] Furthermore, numerous PPAs can cure neuro-psychiatric disorders such as Alzheimer's and Parkinson's diseases.[2] Owing to the importance of PPAs, diverse methods, for example, A^3 coupling reaction, have been improved for their preparation.[3] Among all suggested PPA synthesis approaches, the A^3 coupling method is considered as the most efficient and direct method. In this technique, a homogeneous or heterogeneous transition-metal catalyst is used for coupling the three reaction components, that is, an amine, an aldehyde, and a terminal alkyne.[4] In recent years, diverse homogeneous and heterogeneous catalysts have been applied to synthesize PPA via A^3-coupling reaction based on transition metals containing Zr^{4+},[5] Mn^{2+},[6] Re^{1+},[7] Fe^{2+},[8] Ru^{3+},[9] Co^{2+},[10] Ir^{1+},[11] Ni^{2+},[12] Pd^{2+},[13] Cu^{2+},[14] Ag^{1+},[15] Au^{0},[16] Zn^{2+},[17] Cd^{2+},[18] and Hg^{2+}.[19] The used transition-metal catalysts can be in the form of nanoparticles (NPs) resulting in a great surface-to-volume ratio, excellent selectivity, and good activity for the coupling reaction.[20,21]

The NPs can be a more attractive option if they are magnetic as magnetic NPs (MNPs) ease elimination and recovery of nanocatalysts from reaction mixtures.[22] Diverse core-/shell-structured MNPs have been applied to reduce the cost of catalyzed reactions.[23−28] However, Fe_3O_4-based core/shell NPs have been the most extensively used nanocatalysts because of their ease in magnetic separation and noticeable catalytic activity. Importantly, Fe_3O_4 systems can be functionalized with numerous functional groups for carrying noble metals. In this regard, polymers are a suitable option as they can tolerate a large number of functional groups in their chains for presenting excellent compatibility with the interest metals. The other benefit of anchoring polymers on Fe_3O_4 MNPs is that the existence of the polymers avoids accumulation of the magnetic core/shell structures, which is a common issue in preparing Fe_3O_4 core/shell nanocatalysts. For this reason, numerous studies have emphasized on the encapsulation of Fe_3O_4 NPs by diverse polymers. Several examples of the reported Fe_3O_4−polymer composites are Fe_3O_4@polypyrrole, Fe_3O_4@polyaniline, and Fe_3O_4@polydoapmine, which have shown excellent catalytic potential.[29−32]

Received: June 11, 2019
Accepted: August 1, 2019
Published: August 15, 2019

DOI: 10.1021/acsomega.9b01720
ACS Omega 2019, 4, 13991−14003

As stated, polymer−iron oxide composites have the ability to carry noble metals. The metal which is of interest in the current research is silver. So far, numerous investigations have reported the synthesis of Ag NPs for different purposes. As an example, Ag NPs have been used as extremely active surface-enhanced Raman scattering substrates,[33] electrochemical and biosensors,[34,35] antibacterial coatings,[36] and extremely effective catalysts of organic reactions.[37] As catalysts, Ag NPs have been used in oxidation of phenylsilanes, alcohol dehydrogenation, Diels−Alder cycloadditions, and reduction of aromatic compounds.[38−40] Although the inadequacy of Ag NPs is that their surface atoms destabilize over reactions. Opportunely, immobilization of the Ag NPs onto supports can overcome this problem.[41,42] In the current research, the support material is polymer-immobilized MNPs because of their various advantages. As mentioned above, one of the key advantages of using MNPs is that their supermagnetic and insoluble features allow the isolation of MNP-supported noble metals from reaction mixtures by means of an appropriate magnet and with no need of filtration or centrifugation. Moreover, immobilizing Ag NPs onto the surface of polymer−Fe_3O_4 particles develops dispersing Ag NPs and their ability to promote biological separation, biological targeting, catalysis, high-density magnetic recording, and targeting treatment.[43]

Regarding the wide variety of Ag−Fe_3O_4 applications, numerous approaches have been developed for their preparation. Zhang et al. studied the one-pot water-phase preparation of Ag−Fe_3O_4 MNPs with the $FeCl_3$ and $AgNO_3$ metal precursors and the ethylene glycol reductant.[44] Using the same technique, Zhu et al. synthesized Ag−Fe_3O_4 MNPs in the presence of polyvinylpyrrolidone.[45] Chen et al. used a solvothermal technique to attain Ag/Fe_3O_4 nanowires. In their research, a polyol synthesis method was used to prepare Ag nanowires and Fe_3O_4 particles were coated on the wires via the solvothermal technique.[46] Lopes et al. prepared Ag−Fe_3O_4 colloidal dimer NPs via a two-step chemical technique. First, they synthesized Ag NPs by heating a phenyl-ether solution of oleyamine, oleic acid, and $C_{54}H_{45}NO_3P_3Ag$ at a temperature of 250 °C. Then, the obtained phenyl-ether mixture containing colloidal Ag NPs, $Fe(acac)_3$, oleic acid, 1,2-hexadecanediol, and oleyamine was heated to obtain heterodimer Ag−Fe_3O_4 NPs.[47] Li et al. utilized an electroless silver plating method to synthesize Ag/Fe_3O_4 MNPs via bringing a solution of $AgNO_3$ and formaldehyde (methanal) in contact with Fe_3O_4 NPs.[48] The point is that these introduced preparation methods have numerous disadvantages such as operation at high temperatures and pressures, comprising complex chemical preparation, and using expensive surfactants. Consequently, these approaches should be substituted with an alternative simple, fast, and low-cost method, such as plant-mediated NP preparation. This biosynthesis method is a cost-effective and single-step method that needs nontoxic reagents and environmental friendly solvents. Accordingly, this technique is safe for humans and the environs.[49−55]

In the current study, the *Rubia tinctorum* plant (Figure 1) is selected for biosynthesizing the MNPs. This plant belongs to the Rubiaceae family, which has 6000 species and 500 genera,[56] and is named "madder" in English and "ronas" in Persian.[57] Over all, this plant has been originated from Caucasus and Near East; however, it is cultivated in the north of Africa, the Mediterranean regions from Spain to Asia, and, moreover, in some regions of Asia. In Iran, it is planted in some central and western regions, for example, Yazd.[58] This plant

Figure 1. *R. tinctorum* image.

comprises numerous anthraquinones containing rubiadin, purpurin, lucidin, and alizarin.[59−63]

Today, ecological concerns have encouraged chemists to shift toward green chemistry.[64] Therefore, recoverable heterogeneous catalysts can involve in eliminating or reducing chemical wastes, mainly in the case of large-scale and industrial processes.[65] Regarding the outlined topics and in continuation of our research in this area,[66] this research emphasizes on preparation of PPAs through A^3 coupling of amines, aldehydes, and alkynes, from a green perspective. The suggested synthetic method is catalyzed by the Ag NPs supported on the ultrafine surface-modified Fe_3O_4 MNPs. In this technique, the *R. tinctorum* extract is used as a stabilizer and a reductant agent that modifies the surface of the magnetic Fe_3O_4 NPs. The key advantage of the used Fe_3O_4@*R. tinctorum*/Ag nanocomposite is that it can be recovered and reused several runs with no remarkable loss of performance.

RESULTS AND DISCUSSION

The current research emphasizes on a green and environmental friendly technique that uses a plant extract to modify MNPs for fabricating a novel adsorbent for adsorbing metal ions and reducing them to stabilized metal NPs. The used extract is the *R. tinctorum* extract, which can deposit Ag^+ ions onto the Fe_3O_4 MNPs surface, reduce the ions to Ag NPs, and stabilize the reduced particles effectively. It is worth noting that the biomolecules of *R. tinctorum* have a significant tenacity against accumulation of the Fe_3O_4 MNPs, besides reducing silver salts strongly. Moreover, the phenolic compounds of the *R. tinctorum* extract consist of hydroxyl and ketonic groups that can connect to metals and show chelating impact. In the current research, the NPs of Fe_3O_4@*R. tinctorum*/Ag were prepared via the two-stage modification of iron oxide (Fe_3O_4) MNPs using the *R. tinctorum* extract and, then, adsorbing Ag^+ ions onto the modified MNPs and reducing and stabilizing the adsorbed ions by the extract. One of the benefits of this preparation method is reducing the dimension of the MNPs from 15−20 to 2−5 nm, as the adsorbed extract can reduce and stabilize the adsorbed Ag^+ ions to Ag NPs, in situ (Scheme 1). After preparation of the Fe_3O_4@*R. tinctorum*/Ag MNPs, the particles were collected using an external magnet. Atomic absorption spectroscopy showed that the Fe_3O_4@*R. tinctorum*/Ag nanocomposite comprises 0.105 mmol g^{-1} of silver. The structure of the nanocatalyst was characterized using diverse analytical methods of X-ray diffraction (XRD), high-resolution transmission electron microscopy (HRTEM), field emission scanning electron microscopy (FESEM), energy-dispersive X-ray (EDX) spectroscopy, inductively coupled plasma atomic emission spectroscopy (ICP-AES), X-ray photoelectron spectroscopy (XPS), vibrating sample magnetometry (VSM), and Fourier-transform infrared (FT-IR) spectroscopy.

FT-IR spectroscopy was performed to assess the variations in the structure of the Fe_3O_4 NPs upon modifying with the extract and formation of Fe_3O_4@*R. tinctorum*/Ag. Figure 2

DOI: 10.1021/acsomega.9b01720
ACS Omega 2019, 4, 13991−14003

Scheme 1. Schematic Fabrication of Fe_3O_4@*R. tinctorum*/Ag NPs Nanocatalyst

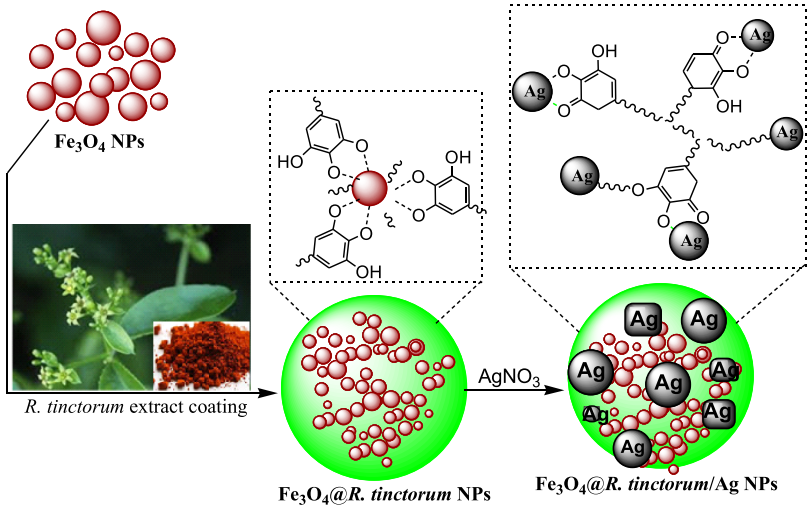

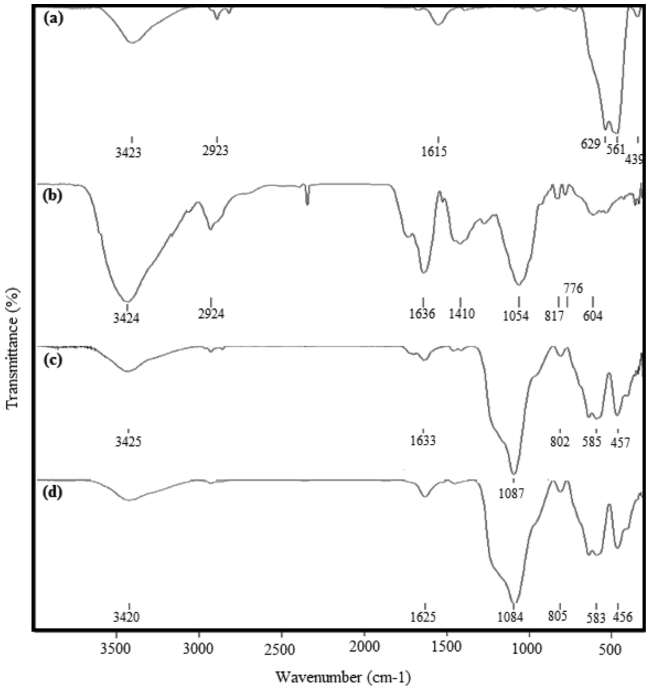

Figure 2. FT-IR spectrum of (a) Fe_3O_4, (b) *R. tinctorum* extract, (c) Fe_3O_4@*R. tinctorum* NPs, and (d) Fe_3O_4@*R. tinctorum*/Ag NPs.

shows the FT-IR spectra corresponding to the Fe_3O_4 NPs, the *R. tinctorum* extract, the Fe_3O_4@*R. tinctorum* MNPs, and the Fe_3O_4@*R. tinctorum*/Ag nanocomposite. On the basis of Figure 2a, the FT-IR spectrum corresponding to the Fe_3O_4 NPs shows two broad peaks at 1615 and 3423 cm^{-1} corresponding to the adsorbed water molecules and the OH groups; however, the bands observed at 439 and 581 cm^{-1} are associated with the bending and stretching vibrations of the Fe−O function group, respectively, and the band at 629 cm^{-1} confirms the presence of a pure Fe_3O_4 structure. On the other hand, the FT-IR spectrum corresponding to the aqueous *R. tinctorum* extract (Figure 2b) shows the 3424 (OH), 2924 (C−H), 1718 (CO), 1636 (C═C), 1285 (C−O), 1054 (C−O−C), and 815 cm^{-1} (O−H) vibrational modes that are related to polyols, carbonyls, and C═C bonds and propose the existence of flavonoids and terpenoids in the extract. When the Fe_3O_4 NPs are functionalized by the extract, that is, the Fe_3O_4@*R. tinctorum* NPs, the related FT-IR spectrum (Figure 2c) is accompanied with several new vibrational bands that are not found in Figure 1a,b. These bands are directly resulted by coating the NPs with the extract's compounds and appeared at 1723 and 1087 cm^{-1} corresponding to the stretching vibrations of the C═O and C−O bonds, respectively,[67] and the bands appeared at 2924 and 2887 cm^{-1} rising from the C−H stretching vibrations.[68] Moreover, numerous bands have been observed at 1400−1600 cm^{-1} that are ascribed to the stretching vibrations of C═C bonds in aromatics rings.[69] These bands show that the hydrophilic nature of the modified NP surface because of the effective coating of the *R. tinctorum* extract on the Fe_3O_4 NPs surface. Finally, the FT-IR spectrum corresponding to the Fe_3O_4@*R. tinctorum*/Ag NPs (Figure 2d) is the same as that of the Fe_3O_4@*R. tinctorum* NPs. However, as it can be observed, the 1087 cm^{-1} band of the C−O stretching vibration is moved to 1084 cm^{-1}, the C═C stretching band is shifted from 1633 to 1625 cm^{-1}, and the O−H stretching band is moved from 3425 to 3420 cm^{-1}. These shifts show that the extract components are chemically bonded to the Ag NPs on the MNP surface. According to the achieved spectra, the hydroxyl functional groups corresponding to the flavonoids and other phenolic compounds of the extract are the active moieties that cause reduction of the adsorbed Ag^+ ions to Ag^0 and stabilization of the Ag NPs. Actually, because of the antioxidant nature of flavonoids and phenolic compounds, donating an electron (accompanied with a hydrogen nucleus) from the OH groups of the phenolic rings should be involved in reducing Ag^+ ions to Ag^0.[70]

The shape, distribution of size, surface morphology, and major physical features of the produced particles were assessed using FESEM. Because the FESEM images of the Fe_3O_4 and Fe_3O_4@*R. tinctorum*/Ag MNPs (Figure 3) show that the Fe_3O_4 particle size in the Fe_3O_4@*R. tinctorum*/Ag MNPs is smaller compared to the initial Fe_3O_4 particles while both specimens consist quasi-spherical NPs, it is obvious that coating Fe_3O_4 NPs with the extract causes a significant decrease in its particle size. Furthermore, the considerable difference between the Ag NPs and the iron oxide particles in Figure 3b shows that the Ag^+ ions have been effectively decreased in situ for immobilizing Ag NPs onto the Fe_3O_4@*R. tinctorum* NP surface. Furthermore, the FESEM images display

DOI: 10.1021/acsomega.9b01720
ACS Omega 2019, 4, 13991−14003

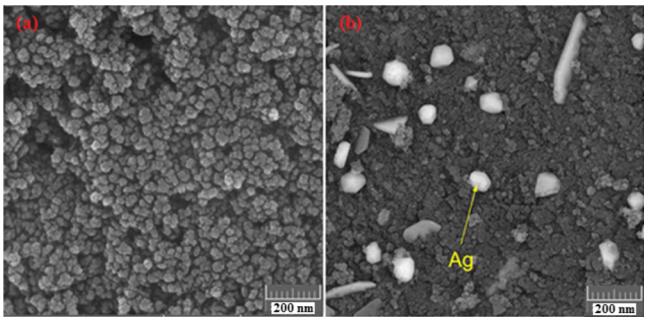

Figure 3. FE-SEM images of (a) Fe_3O_4 and (b) Fe_3O_4@*R. tinctorum*/Ag NPs.

that both the Ag and iron oxide NPs have crystalline structures with dimension ranging in 20−40 and 2−5 nm, respectively.

Figure 4 demonstrates the elemental composition corresponding to the magnetic samples. According to the achieved

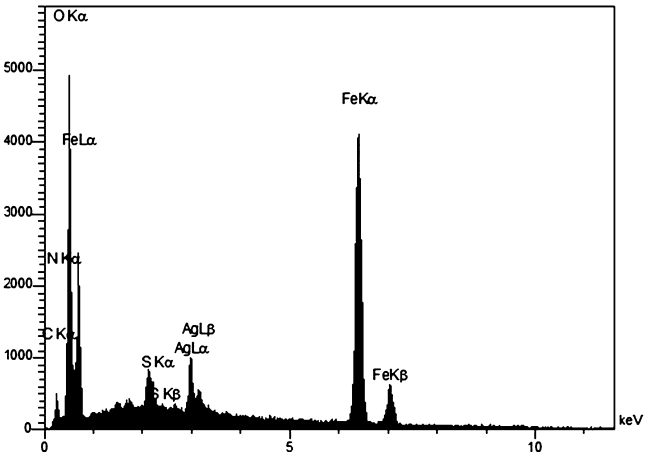

Figure 4. EDX of the Fe_3O_4@*R. tinctorum*/Ag NPs.

EDX outcomes, silver species are dispersed on the extract shell homogeneously and the Fe_3O_4 NPs have been fully coated with the extract. Furthermore, the Fe, C, N, S, O, and Ag elements are in the Fe_3O_4@*R. tinctorum*/Ag nanocatalyst. The S signal that represents the alizarin molecules of the *R. tinctorum* extract approves effective modification of the Fe_3O_4 NPs using the extract while the presence of the Ag signal confirms successful functionalization of Ag NPs and synthesis of the desired Fe_3O_4@*R. tinctorum*/Ag NPs. Also, its elemental maps are displayed in Figure 5, which confirmed the well-dispersed Ag NPs in the sample.

Moreover, the morphology of the as-prepared NPs was analyzed using HRTEM. Comparing the HRTEM images corresponding to the Fe_3O_4 (Figure 6a), Fe_3O_4@*R. tinctorum* (Figure 6b), and Fe_3O_4@*R. tinctorum*/Ag (Figure 6c) NPs unravels that the spherical Fe_3O_4 cores of the Fe_3O_4@*R. tinctorum*/Ag and Fe_3O_4@*R. tinctorum* MNPs are very smaller compared to the initial Fe_3O_4 particles and the magnetic cores are well distributed following coating them with the biocomponents of the *R. tinctorum* extract. It seems that the appeared thin layer of biomolecules on the Fe_3O_4@*R. tinctorum* particles is responsible for reduction and stabilization of silver on the magnetic support. Moreover, comparison of Figure 6b and c shows the existence of the functionalized Ag NPs on the Fe_3O_4 MNP surface and proposes that the Ag NPs are almost 20−40 nm in scale within a narrow size distribution. The agreement of the HRTEM and FESEM outcomes leaves no doubt about the ability of the *R. tinctorum* layer of Fe_3O_4@*R. tinctorum* in reduction and deposition of Ag NPs with an excellent particle distribution on the MNPs surface. Figure 6d shows the HRTEM image corresponding to the Ag NPs at 5 nm magnification. On the basis of Figure 6d, the Ag NPs include lattice fringes, which confirm the excellent crystallinity of these NPs. Meanwhile, the fast Fourier transform (FFT) image corresponding to the Ag NPs (Figure 6e) shows bright diffraction spots and ring patterns that signify the crystalline structure of the Ag atoms on the surface of Fe_3O_4@*R. tinctorum*.

Besides confirming the deposition of Ag NPs onto the Fe_3O_4@*R. tinctorum* surface using the FESEM and HRTEM methods, the nanocatalyst was studied using XRD analysis to additionally approve the coated particles and unravel their crystal features. The obtained XRD patterns corresponding to the Fe_3O_4 and Fe_3O_4@*R. tinctorum*/Ag NPs are shown in Figure 7. The (220), (311), (400), (422), (511), and (440) crystal planes of the Fe_3O_4 NPs indicate the cubic structures of Fe_3O_4 MNPs (JCPDS no. 19-0629). However, these crystal planes also appeared in the XRD pattern corresponding to Fe_3O_4@*R. tinctorum*/Ag; the additional bands observed at 38.2° (111), 44.3° (200), 64.5° (220), and 78.2° (311) show that the cubic magnetite crystals are combined with face-centered cubic silver crystals (JCPDS no. 87-720). This evidence approves effective synthesis of the Ag NPs on the surface of Fe_3O_4@*R. tinctorum* MNPs. The last point of the crystal structures of the synthesized NPs is that the surface functionalization and silver deposition procedures are unsuccessful on the crystal structure of the Fe_3O_4 NPs. Thus, the specific XRD bands of the pristine Fe_3O_4 NPs also appear in the XRD pattern corresponding to the Fe_3O_4@*R. tinctorum*/Ag NPs.

The electronic features of the surface species of the MNPs containing their oxidation states, electron environs, and binding energies (BEs) were examined using XPS. Figures 8

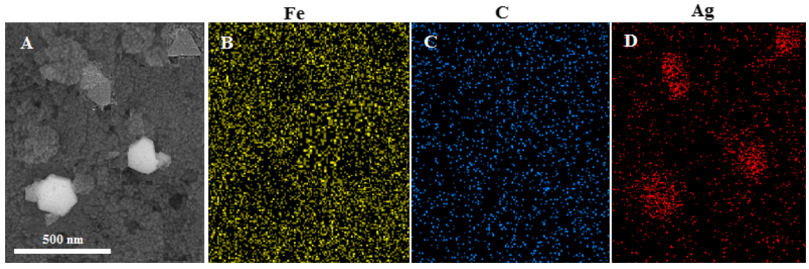

Figure 5. (A−D) Corresponding elemental mapping of Fe_3O_4@*R. tinctorum*/Ag NPs, Fe, C, and Ag, respectively (scale bar is 500 nm).

DOI: 10.1021/acsomega.9b01720
ACS Omega 2019, 4, 13991−14003

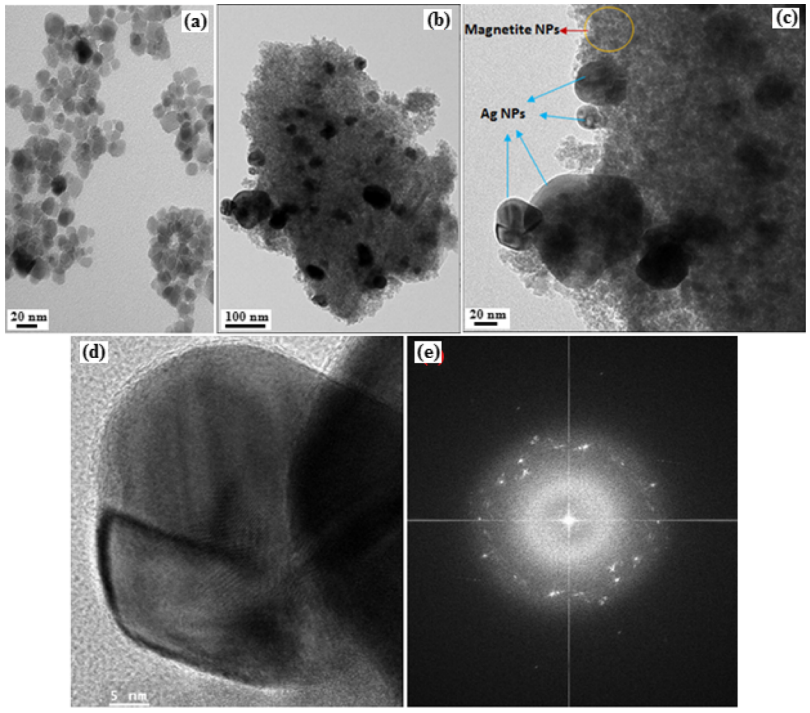

Figure 6. HRTEM images of the as-prepared Fe_3O_4 NPs (a), Fe_3O_4@*R. tinctorum*/Ag NPs (b,c), HRTEM image of Ag NPs at 5 nm (d), and FFT image of Ag NPs corresponding to image of (d) (e).

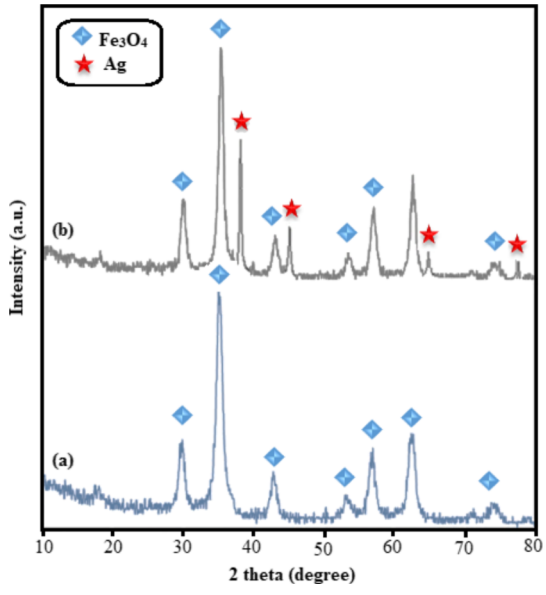

Figure 7. XRD patterns of (a) Fe_3O_4 and (b) Fe_3O_4@*R. tinctorum*/Ag nanocomposites.

and 9 show the XPS elemental scans for the Fe_3O_4@*R. tinctorum*/Ag nanocatalyst. In agreement with the EDX outcomes, the XPS spectra show the existence of oxygen, carbon, nitrogen, silver, and iron. Moreover, the XPS outcomes show an intense doublet at the 374.33 and 368.32 eV BEs, which imply the Ag $3d_{3/2}$ and Ag $3d_{5/2}$ bands, respectively. The XPS outcomes show the presence of reduced Ag(0) species and exclude the possibility of +1 oxidation state for the coated Ag NPs. The well reduction of Ag(I) to Ag(0) approves the efficiency of the *R. tinctorum* layer.[71]

In Figure 9, the characteristic bands of carbon (C 1s) and iron (Fe 2p) are obvious, which shows that the *R. tinctorum* extract is effectively deposited on the iron oxide MNPs. The XPS spectrum corresponding to Fe 2p displays two key bands that are associated with Fe $2p_{3/2}$ and Fe $2p_{1/2}$ and can be deconvoluted to the 712.4, 715.8, 719.3, 726.5, 729.8, and 733.4 eV bands. Four of these bands refer to Fe^{2+} (712.4 and 726.5 eV) and Fe^{3+} (715.8 and 729.8 eV) in the Fe_3O_4 phase while the two satellite bands (719.3 and 733.4 eV) relate with Fe^{3+} in the Fe_2O_3 phase. In other words, the study of the oxidation states points to the presence of few γ-Fe_2O_3 particles.[72−74] Finally, fitting of the C 1s XPS spectra corresponding to the Fe_3O_4@*R. tinctorum*/Ag nanocatalyst shows nonoxygenated carbon at 285.2 eV, carbon in C−OH/C−O−C at 288.2 eV, carbon in C═O at 289.2 eV, and the O−C═O group at 292.7 eV. Also, the UV analysis of the Fe_3O_4@*R. tinctorum*/Ag NPs is demonstrated in Figure 10a. The peak absorption at 418 nm related to Ag NPs, which confirmed the presence of Ag NPs in the Fe_3O_4@*R. tinctorum*/Ag NP nanocamposite.

As the final characterization stage, the magnetic features of the prepared Fe_3O_4 and Fe_3O_4@*R. tinctorum*/Ag NPs were examined with VSM. On the basis of Figure 10b, both of the Fe_3O_4 and Fe_3O_4@*R. tinctorum*/Ag samples show a usual superparamagnetic activity with almost zero remanence and coercivity. Furthermore, the VSM outcomes indicate that adding *R. tinctorum* extract and Ag layers reduces the saturation magnetization (M_s) of the Fe_3O_4 NPs. However, the M_s value for Fe_3O_4@*R. tinctorum*/Ag (40.3 emu/g) is significantly smaller compared with that of the Fe_3O_4 NPs (62.4 emu/g), and the magnetic sensitivity of the Fe_3O_4@*R. tinctorum*/Ag is adequate for its magnetic recovery from diverse reaction mixtures. Consequently, the prepared nanocomposite has the ability to act as a magnetically recoverable nanocatalyst.

Once the Fe_3O_4@*R. tinctorum*/Ag NP structure had been recognized, as a nanocatalyst, the catalytic activity of Fe_3O_4@*R. tinctorum*/Ag NPs was evaluated in the three-component

DOI: 10.1021/acsomega.9b01720
ACS Omega 2019, 4, 13991−14003

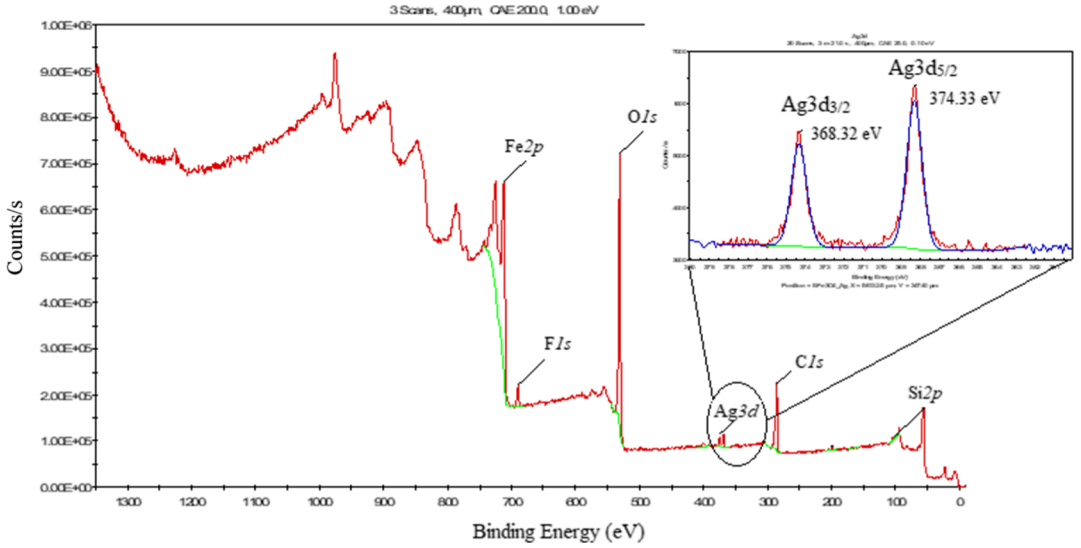

Figure 8. XPS spectrum related to the elemental survey scan of Fe_3O_4@*R. tinctorum*/Ag and in the Ag 3d regions.

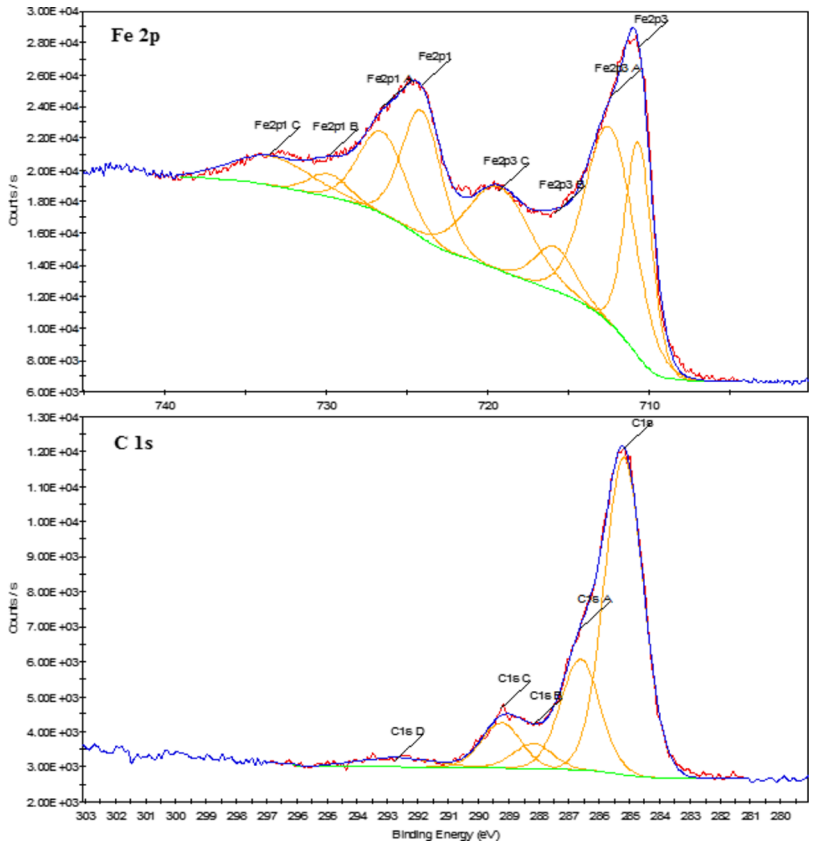

Figure 9. Wide scan XPS spectrum of Fe_3O_4@*R. tinctorum*/Ag and in the Fe 2p and C 1s regions.

coupling reaction of aldehydes, amines, and alkynes (A^3 coupling). Initial experiments using phenylacetylene, morpholine, and benzaldehyde were performed to optimize diverse parameters comprising solvent, time, temperature, and catalyst load. The results are listed in Table 1. First, the impact of catalyst was examined, and as expected, the desired product was not attained with no catalyst offering the vital role of Fe_3O_4@*R. tinctorum*/Ag NPs in the reaction mechanism (Table 1, entry 1). The reaction yield was attained 70% by using a 0.1 mol % catalyst loading in water at a temperature of 50 °C (Table 1, entry 2). Moreover, the reaction took place quantitatively by using 0.1 mol % of catalyst at a temperature of 80 °C (Table 1, entry 3). Smaller yields were attained by reducing the catalyst level to 0.06 and 0.03 mol % (Table 1, entries 4 and 5). However, using 0.03 mol % of catalyst in other solvents containing CH_2Cl_2, dimethylformamide (DMF), EtOH, toluene, CH_3CN, and neat provided smaller reaction performances (Table 1, entries 6−11). There was no change in the reaction time and reaction performance by growing the amount of catalyst or reaction temperature (Table

DOI: 10.1021/acsomega.9b01720
ACS Omega 2019, 4, 13991−14003

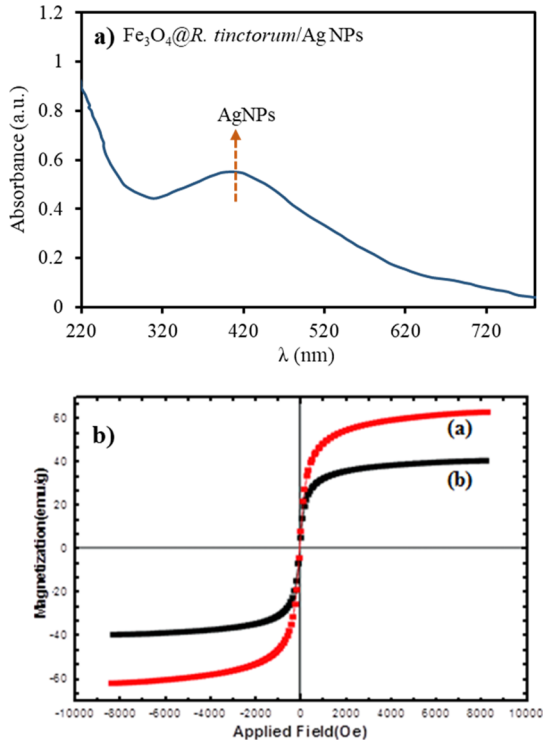

Figure 10. UV−vis spectrum of Fe_3O_4@*R. tinctorum*/Ag NPs (a) and VSM of (a) Fe_3O_4 and (b) Fe_3O_4@*R. tinctorum*/Ag NPs.

Table 1. Optimization of Reaction Parameters for the Model Reaction Using Fe_3O_4@*R. tinctorum*/Ag NPs Catalyst[a]

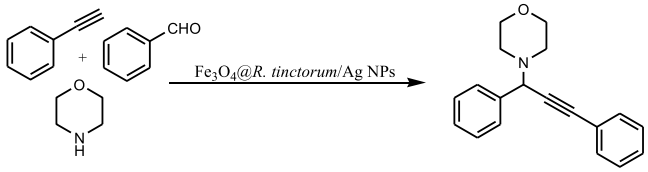

entry	catalyst (mol %)	solvent	T (°C)	time (h)	yield (%)[b]
1		H_2O	50	24	
2	0.1	H_2O	50	12	70
3	0.1	H_2O	80	8	96
4	0.06	H_2O	80	12	60
5	0.03	H_2O	80	24	52
6	0.1	CH_2Cl_2	70	24	30
7	0.1	DMF	100	12	60
8	0.1	EtOH	80	12	45
9	0.1	toluene	100	12	96
10	0.1	CH_3CN	70	12	65
11	0.1		100	12	25
12	0.1	H_2O	100	8	96
13	0.12	H_2O	80	8	96

[a]Reaction conditions: benzaldehyde (1.0 mmol), phenylacetylene (1.2 mmol), morpholine (1 mmol), Fe_3O_4@*R. tinctorum*/Ag NPs, and solvent (3.0 mL). [b]Yields are based on ^{1}H NMR.

1, entries 12 and 13). Therefore, we selected water as a safe and eco-friendly solvent, 0.1 mol % catalyst loading, and reaction temperature of 80 °C as the most efficient and optimal reaction conditions to study the generality of this A^3 coupling.

Under the optimum reaction conditions, diverse aldehydes were interacted with other aliphatic amines and phenylacetylene that provided the A^3 coupling product with excellent yields and good turnover frequencies (TOFs) (Table 2). At the initial research of the aldehyde substrate scope, morpholine and phenylacetylene were applied as model reaction and diverse aldehydes were examined for the A^3-coupling (Table 2, entries 1−20). The results display that aromatic aldehydes activity like functional groups such as −Br, −Cl, −OH, −OMe, or −Me could influence on the A^3-coupling. Furthermore, minor electronic influence was observed that is associated with the reaction of aryl aldehydes with electron-withdrawing groups (Table 2, entries 2−4) and formation of the correlated products in high yields, while replacement of electron-rich groups (Table 2, entries 5−7) on the benzene ring decreased the efficiency and resulted less yields. Moreover, reaction of heterocyclic aldehyde like furan-2-carboxaldehyde or thiophene-2-carbaldehyde with phenylacetylene and morpholine proceeded effectively and the relating PPAs were archived in high yields (Table 2, entries 8 and 9). The aliphatic aldehyde (cyclohexanecarbaldehyde/butanaldehyde) presented high yields under this optimal condition (Table 2, entries 10 and 11). To develop the generality of amine compounds, a mixture containing phenylacetylene−benzaldehyde−amine was chosen, and diverse amines were examined (Table 2, entries 1 and 12−16). The results show that cyclic, heterocyclic (pyrrolidine/morpholine/piperidine), and acyclic (dibenzyl/diethyl) secondary amines resulted in excellent yields of products (Table 2, entries 1 and 12−15). However, no product was obtained by aniline as a substrate (Table 2, entry 16). Curiously, the reaction of aliphatic alkyne 1-octyne, which is typically difficult to activate, reacted well and provided the product in high yield (Table 2, entries 17−20).

The proposed mechanism is demonstrated in Scheme 2. At first, phenyl acetylene molecules due to interaction p-complex attached to the AgNPs immobilized on Fe_3O_4@*R. tinctorum* involving. On the other hand, the aldehyde is condensed with the secondary amine to give an iminium ion. In the next step, the iminium molecules attach to the AgNPs. Finally, coupling between iminium and phenyl acetylene molecules was performed. The catalytic cycle continues until the completion of the reaction.

Recovery of heterogeneous noble catalysts is a very important point. Consequently, the current research is aimed to recycle the catalyst for the reaction system of benzaldehyde, morpholine, and phenylacetylene under the optimal parameter. For this purpose, after compilation of the reaction, the catalyst was separated from the reaction medium by a magnet and washed with H_2O and EtOH twice, and then it was recovered up to seven times without significant decrease in its catalytic performance (Figure 11). This recoverability shows the high stability and turnover of catalyst under working conditions.

Moreover, to study the catalyst heterogeneity, for the A^3 coupling of the above model substrates, a hot filtration test was performed with Fe_3O_4@*R. tinctorum*/Ag NPs under the optimum conditions. The reaction yield of 65% could be attained after 4 h, and then, the catalyst was isolated using an external magnet. No increase in the activity of the product was observed when the reaction was continued for an additional 4 h following the isolation of the catalyst. This outcome proved the heterogeneous property of the synthesized catalyst. The TEM and EDX data (Figure 12) of the catalyst following the seven cycles confirmed the protection of the catalyst's nanostructure.

DOI: 10.1021/acsomega.9b01720
ACS Omega 2019, 4, 13991−14003

Table 2. Reactions of Aldehydes, Amines, and Alkynes in the Presence of Fe_3O_4@*R. tinctorum*/Ag NP Catalyst[a]

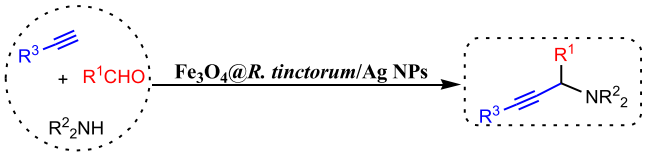

entry	R^1	amine	R^3	yield (%)[b]	TOF (h^{-1})[c]	TON (h^{-1})[d]
1	Ph	morpholine	Ph	96	120	960
2	4-ClC_6H_4	morpholine	Ph	95	118.7	950
3	3-ClC_6H_4	morpholine	Ph	92	115	920
4	4-BrC_6H_4	morpholine	Ph	96	120	960
5	4-OHC_6H_4	morpholine	Ph	90	112.5	900
6	4-MeC_6H_4	morpholine	Ph	88	110	880
7	4-$OMeC_6H_4$	morpholine	Ph	85	106.2	850
8	2-thiophenyl	morpholine	Ph	95	118.7	950
9	2-furfuryl	morpholine	Ph	90	112.5	900
10	cyclohexyl	morpholine	Ph	92	115	920
11	C_3H_7	morpholine	Ph	88	110	880
12	Ph	piperidine	Ph	96	120	960
13	Ph	pyrrolidine	Ph	92	112.5	900
14	Ph	diethyl	Ph	90	112.5	900
15	Ph	dibenzyl	Ph	90	112.5	900
16	Ph	aniline	Ph	0	0	0
17	Ph	morpholine	*n*-C_6H_{13}	85	106.2	850
18	Ph	piperidine	*n*-C_6H_{13}	80	106.2	800
19	4-ClC_6H_4	morpholine	*n*-C_6H_{13}	85	106.2	850
20	4-$OMeC_6H_4$	morpholine	*n*-C_6H_{13}	70	87.5	700

[a]Reaction conditions: aldehyde (1.0 mmol), amine (1 mmol), alkyne (1.2 mmol), and Fe_3O_4@*R. tinctorum*/Ag NPs (10 mg, 0.1 mol %) were stirred in water (3.0 mL) at 80 °C for 8 h. [b]Yields are based on ^{1}H NMR. [c]TOF, turnover frequency (TOF = (yield/time)/amount of catalyst (mol)). [d]TON, turnover number (TON = yield/amount of catalyst (mol)).

Scheme 2. Proposed Mechanism for Synthesis of PPA in the Presence Fe_3O_4@*R. tinctorum*/Ag NP Catalyst

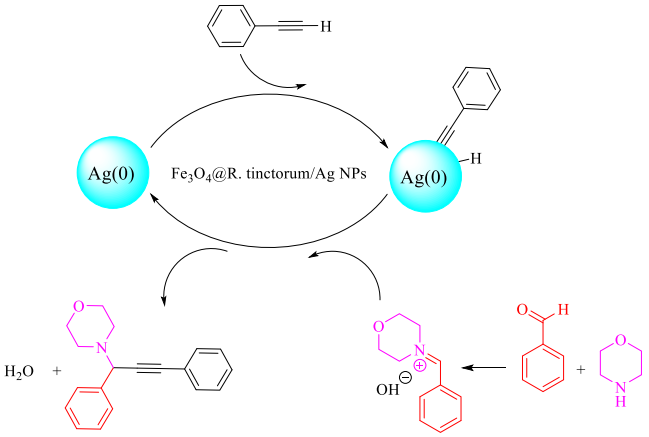

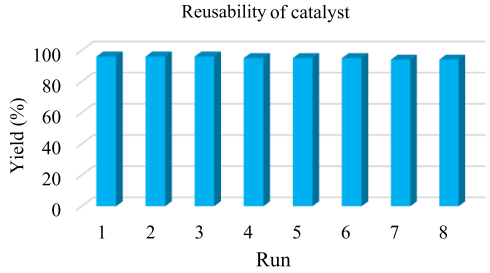

Figure 11. Recycling of the Fe_3O_4@*R. tinctorum*/Ag NP catalyst.

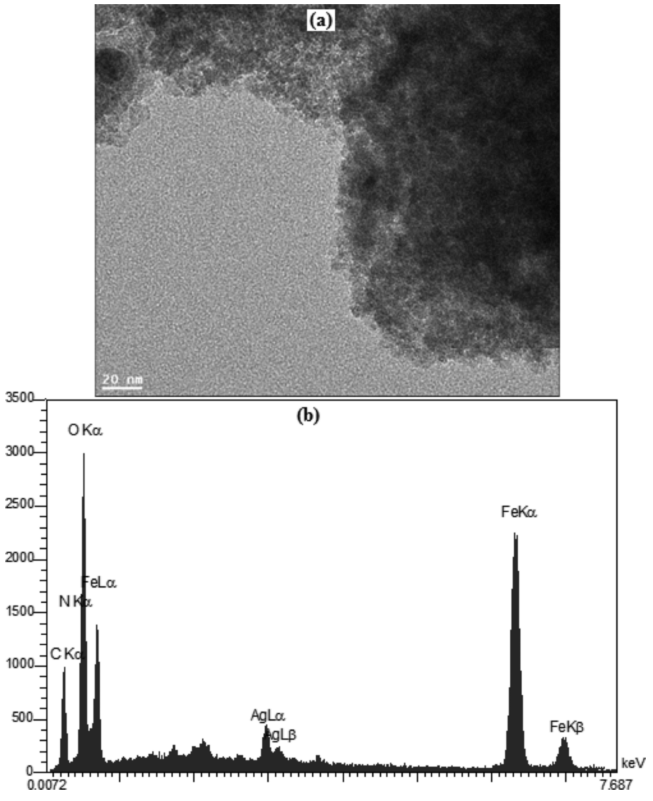

Figure 12. (a) TEM and (b) EDX analysis of reused catalyst after the seventh run.

DOI: 10.1021/acsomega.9b01720
ACS Omega 2019, 4, 13991−14003

Three catalysts were prepared with different loading amounts of Ag % (0.105, 0.29, and 0.44 mmol/g), which resulted in the increase of reaction rate with the increase of Ag in the Fe_3O_4@*R. tinctorum*/Ag composite (Table 3).

Table 3. Effect of Different Loading Amounts of Ag % on the A^3-Coupling Reaction of Benzaldehyde, Morpholine, and Phenylacetylene

entry	Ag loading (mmol/g)	TOF (h^{-1})
1	0.105	120
2	0.29	205
3	0.44	294

To prove the ability of this technique for synthesis purposes, the scale-up production of PPAs was studied with 4-(1,3-diphenylprop-2-ynyl)morpholine (Table 2, entry 1) as a model reaction. The results are shown in Table 4. The A^3-coupling reaction between benzaldehyde, phenylacetylene, and morpholine proceeded successfully, and the product was attained in high yields almost comparable to those in the small-scale reactions. The results of scale-up tests revealed that the purified product yield was 82% if the reaction scale was 100 mmol.

Table 4. Scale-Up Synthesis of the A^3-Coupling Reaction of Benzaldehyde, Morpholine, and Phenylacetylene

entry	scale (mmol)	isolated yield (%)
1	1	96
2	10	94
3	20	90
4	50	85
5	100	82

Numerous selected processes in reports and current process are compared in Table 5, which specify that Fe_3O_4@*R. tinctorum*/Ag NPs are equally or more efficient catalysts in terms of reaction time and yield compared to previously reported ones.

CONCLUSIONS

This research introduced an efficient, easy, green, and economical technique for synthesizing Fe_3O_4@*R. tinctorum* as a metal reductant and stabilizer agent and used it for the preparation of Fe_3O_4@*R. tinctorum*/Ag NPs. The characterization of particles was performed using the FT-IR, SEM, energy-dispersive X-ray spectroscopy (EDS), TEM, XRD, XPS, and VSM methods. The achieved Fe_3O_4@*R. tinctorum*/Ag NPs were reported to be air-stable, economic, and effective for the preparation of PPAs through one-pot three-component A^3-coupling of amines, aldehydes, and alkynes. The products of the A^3-coupling reaction were obtained in good to excellent yields and the catalyst was recovered for seven runs with no loss in its catalytic performance. The main properties of the suggested method do not need homogeneous catalysts, providing high product yields; use of a plant extract as a green and fast synthetic method for modifying MNPs; no need of surfactants, capping agents, or templates; easy immobilization of Ag NPs; and catalyst recoverability.

Table 5. Comparison Efficiency of Fe_3O_4@*R. tinctorum*/Ag NPs with Some Reported Methods for the A^3 Coupling Reaction (Phenylacetylene/Benzaldehyde/Piperidine)

entry	reaction conditions	temp. (°C)	TOF (h^{-1})	yield %
1	Fe_3O_4@*R. tinctorum*/Ag NPs, H_2O	80	120	this work
2	AgI, H_2O, N_2	100	3.3	76
3	Ag NPs, PEG	100	1.92	81
4	Ag−NaY, neat	100	0.97	82
5	Ag−CIN-1, H_2O	40	2.72	16c
6	ZnO-IL/Ag, H_2O, 3 h	reflux	51.1	83
7	PS-NHC-Ag(1), solvent	RT	4	84
8	g-C_3N_4/Ag(0), EtOH/H_2O, microwave	80	245	85

EXPERIMENTAL SECTION

Materials and Apparatus. This part is according to our previously work.[86]

Preparations of Fe_3O_4@*R. tinctorum* by *R. tinctorum* Extract. *R. tinctorum* powder (0.5 g, Ronas) was poured into 50 ml of Milli-Q water and agitated at a temperature of 50 °C for 20 min. Next, the extract was filtered through Whatman no. 1 filter paper and centrifuged at 4000 rpm for 5 min to separate unwanted aggregates. The filtered extract is utilized for the following phase.

For the preparation of Fe_3O_4@*R. tinctorum* NPs in the first stage, magnetite NP (500 mg) was distributed in 100 mL of water and sonicated for 20 min. Then, the *R. tinctorum* extract was poured into the mixture. Subsequently, the solution was agitated for 3 days at ambient temperature, and then, the Fe_3O_4@*R. tinctorum* NPs precipitate achieved was isolated by magnetic decantation and washed several times with deionized water. Finally, it is dried in a vacuum oven at 40 °C for 12 h.

Preparation of the Fe_3O_4@*R. tinctorum*/Ag NPs. The Fe_3O_4@*R. tinctorum* NPs (500 mg) were distributed in deionized water (200 mL) via sonication for 30 min. Then, a solution containing $AgNO_3$ (30 mg) in 20 mL of H_2O was poured into dispersion and the solution was agitated for 5 h at ambient temperature to guarantee full reduction of Ag(I) ions in the precursor solution. Next, the Fe_3O_4@*R. tinctorum*/Ag NPs were isolated by magnetic decantation and rinsed with H_2O and acetone to eliminate the unattached substrates. Scheme 1 showed the synthetic process of Fe_3O_4@*R. tinctorum*/Ag NPs. The last nanocatalyst was dried in vacuum at a temperature of 40 °C. The amount of silver was 0.105 mmol/g, which was measured by ICP-AES.

General Procedure for the Synthesis of PPAs Using Fe_3O_4@*R. tinctorum*/Ag NPs. The Fe_3O_4@*R. tinctorum*/Ag catalyst (10 mg, 0.1 mol %) was added to the mixture of aldehyde (1 mmol), phenylacetylene (1.2 mmol), and amine (1 mmol) in H_2O (3 mL) and the mixture was agitated at a temperature of 80 °C. At the end of the reaction, the catalyst was isolated using a magnet, rinsed with ethanol, and dried for another cycle. The product mixtures were isolated with EtOAc and concentrated to obtain the crude product. In the next step, the crude product was purified using a silica gel column chromatography (70:30, hexane/EtOAc). All compounds were identified and characterized using spectral analysis or melting points.[74−85]

AUTHOR INFORMATION

Corresponding Author
*E-mail: hojatveisi@yahoo.com.

DOI: 10.1021/acsomega.9b01720
ACS Omega 2019, 4, 13991−14003

ORCID

Hojat Veisi: 0000-0003-2038-143X

Notes

The authors declare no competing financial interest.

■ ACKNOWLEDGMENTS

The authors are thankful to Payame Noor University, Tehran, Iran, for financial supports.

■ REFERENCES

(1) (a) Liu, Y. Recent advances on diversity-oriented heterocycle synthesis via multicomponent tandem reactions based on A^3-coupling. *ARKIVOC* **2013**, *2014*, 1−20. (b) Vessally, E. A new avenue to the synthesis of highly substituted pyrroles: synthesis from N-propargyl-amines. *RSC Adv.* **2016**, *6*, 18619−18631. (c) Sar, C. P. T.; Kalai, T.; Jeko, J.; Hideg, K. *ARKIVOC* **1991**, *32*, 47.

(2) (a) Yu, P. H.; Davis, B. A.; Boulton, A. A. Aliphatic propargylamines: potent, selective, irreversible monoamine oxidase B inhibitors. *J. Med. Chem.* **1992**, *35*, 3705−3713. (b) Baranyi, M.; Porceddu, P. F.; Gölöncsér, F.; Kulcsár, S.; Otrokocsi, L.; Kittel, Á.; Pinna, A.; Frau, L.; Huleatt, P. B.; Khoo, M. L.; Chai, C. L. Novel (Hetero) arylalkenyl propargylamine compounds are protective in toxin-induced models of Parkinson's disease. *Mol. Neurodegener.* **2016**, *11*, 6−27.

(3) (a) Magueur, G.; Crousse, B.; Bonnet-Delpon, D. Direct access to CF3-propargyl amines and conversion to difluoromethyl imines. *Tetrahedron Lett.* **2005**, *46*, 2219−2221. (b) Kaur, P.; Shakya, G.; Sun, H.; Pan, Y.; Li, G. Chiral N-phosphonyl imine chemistry: an efficient asymmetric synthesis of chiral N-phosphonyl propargylamines. *Org. Biomol. Chem.* **2010**, *8*, 1091−1096.

(4) (a) Hosseini-Sarvari, M.; Moeini, F. Nano copper(I) oxide−zinc oxide catalyzed coupling of aldehydes or ketones, secondary amines, and terminal alkynes in solvent-free conditions. *New J. Chem.* **2014**, *38*, 624−635. (b) Peshkov, V. A.; Pereshivko, O. P.; Van der Eycken, E. V. A walk around the A^3-coupling. *Chem. Soc. Rev.* **2012**, *41*, 3790−3807. (c) Moghaddam, F. M.; Ayati, S. E.; Hosseini, S. H.; Pourjavadi, A. Gold immobilized onto poly(ionic liquid) functionalized magnetic nanoparticles: a robust magnetically recoverable catalyst for the synthesis of propargylamine in water. *RSC Adv.* **2015**, *5*, 34502−34510. (d) Kumar, B. S.; Dhakshinamoorthy, A.; Pitchumani, K. K10 montmorillonite clays as environmentally benign catalysts for organic reactions. *Catal. Sci. Technol.* **2014**, *4*, 2378−2396.

(5) Akullian, L. C.; Snapper, M. L.; Hoveyda, A. H. Three-component enantioselective synthesis of propargylamines through Zr-catalyzed additions of alkyl zinc reagents to alkynylimines. *Angew. Chem., Int. Ed.* **2003**, *42*, 4244−4247.

(6) Afraj, S. N.; Chen, C.; Lee, G.-H. Manganese (II) chloride catalyzed highly efficient one-pot synthesis of propargylamines and fused triazoles via three-component coupling reaction under solvent-free condition. *RSC Adv.* **2014**, *4*, 26301−26308.

(7) Kuninobu, Y.; Inoue, Y.; Takai, K. Rhenium-catalyzed addition of trimethylsilylacetylene to aldimines. *Chem. Lett.* **2006**, *35*, 1376−1377.

(8) (a) Kotadia, D. A.; Soni, S. S. Stable mesoporous Fe/TiO_2 nanoparticles: A recoverable catalyst for solvent-free synthesis of propargylamine via CH activation. *Appl. Catal., A* **2014**, *488*, 231−238. (b) Zeng, T.; Chen, W.-W.; Cirtiu, C. M.; Moores, A.; Song, G.; Li, C.-J. Fe_3O_4 nanoparticles: a robust and magnetically recoverable catalyst for three-component coupling of aldehyde, alkyne and amine. *Green Chem.* **2010**, *12*, 570−573.

(9) Li, C.-J.; Wei, C. Highly efficient Grignard-type imine additions via C−H activation in water and under solvent-free conditions. *Chem. Commun.* **2002**, 268−269.

(10) Chen, W.-W.; Bi, H. P.; Li, C. J. The First Cobalt-Catalyzed Transformation of Alkynyl CH Bond: Aldehyde-Alkyne-Amine (A^3) Coupling. *Synlett* **2010**, 475−479.

(11) (a) Sakaguchi, S.; Kubo, T.; Ishii, Y. A Three-Component Coupling Reaction of Aldehydes, Amines, and Alkynes. *Angew. Chem., Int. Ed.* **2001**, *40*, 2534−2536. (b) Sakaguchi, S.; Mizuta, T.; Furuwan, M.; Kubo, T.; Ishii, Y. Iridium-catalyzed coupling of simple primary or secondary amines, aldehydes and trimethylsilylacetylene: preparation of propargylic amines. *Chem. Commun.* **2004**, 1638−1639.

(12) Samai, S.; Nandi, G. C.; Singh, M. S. An efficient and facile one-pot synthesis of propargylamines by three-component coupling of aldehydes, amines, and alkynes via C−H activation catalyzed by $NiCl_2$. *Tetrahedron Lett.* **2010**, *51*, 5555−5558.

(13) Manikandan, R.; Anitha, P.; Viswanathamurthi, P.; Malecki, J. G. Palladium (II) pyridoxal thiosemicarbazone complexes as efficient and recyclable catalyst for the synthesis of propargylamines by a three-component coupling reactions in ionic liquids. *Polyhedron* **2016**, *119*, 300−306.

(14) (a) Cheng, S.; Shang, N.; Feng, C.; Gao, S.; Wang, C.; Wang, Z. Efficient multicomponent synthesis of propargylamines catalyzed by copper nanoparticles supported on metal-organic framework derived nanoporous carbon. *Catal. Commun.* **2017**, *89*, 91−95. (b) Varyani, M.; Khatri, P. K.; Jain, S. L. Amino acid ionic liquid bound copper Schiff base catalyzed highly efficient three component A^3-coupling reaction. *Catal. Commun.* **2016**, *77*, 113−117. (c) Islam, M. M.; Roy, A. S.; Islam, S. M. Functionalized polystyrene supported copper (I) complex as an effective and reusable catalyst for propargylamines synthesis in aqueous medium. *Catal. Lett.* **2016**, *146*, 1128−1138. (d) Kumari, S.; Shekhar, A.; Pathak, D. D. Synthesis and characterization of a Cu (II) Schiff base complex immobilized on graphene oxide and its catalytic application in the green synthesis of propargylamines. *RSC Adv.* **2016**, *6*, 15340−15344. (e) Gholinejad, M.; Saadati, F.; Shaybanizadeh, S.; Pullithadathil, B. Copper nanoparticles supported on starch micro particles as a degradable heterogeneous catalyst for three-component coupling synthesis of propargylamines. *RSC Adv.* **2016**, *6*, 4983−4991.

(15) (a) Wei, C.; Li, Z.; Li, C.-J. The first silver-catalyzed three-component coupling of aldehyde, alkyne, and amine. *Org. Lett.* **2003**, *5*, 4473−4475. (b) Li, P.; Wang, L.; Zhang, Y.; Wang, M. Highly efficient three-component (aldehyde−alkyne−amine) coupling reactions catalyzed by a reusable PS-supported NHC−Ag (I) under solvent-free reaction conditions. *Tetrahedron Lett.* **2008**, *49*, 6650−6654. (c) Li, Z.; Wei, C.; Chen, L.; Varma, R. S.; Li, C.-J. Three-component coupling of aldehyde, alkyne, and amine catalyzed by silver in ionic liquid. *Tetrahedron Lett.* **2004**, *45*, 2443−2446. (d) Salam, N.; Kundu, S. K.; Molla, R. A.; Mondal, P.; Bhaumik, A.; Islam, S. M. Ag-grafted covalent imine network material for one-pot three-component coupling and hydration of nitriles to amides in aqueous medium. *RSC Adv.* **2014**, *4*, 47593−47604.

(16) (a) Gholinejad, M.; Hamed, F.; Najera, C. Gold nanoparticles supported on polyacrylamide containing a phosphorus ligand as an efficient heterogeneous catalyst for three-component synthesis of propargylamines in water. *Synlett* **2016**, *27*, 1193−1201. (b) Veisi, H.; Farokhi, M.; Hamelian, M.; Hemmati, S.; Hemmati, S. Green synthesis of Au nanoparticles using an aqueous extract of Stachys lavandulifolia and their catalytic performance for alkyne/aldehyde/amine A 3 coupling reactions. *RSC Adv.* **2018**, *8*, 38186−38195. (c) Wei, C.; Li, C.-J. A highly efficient three-component coupling of aldehyde, alkyne, and amines via C− H activation catalyzed by gold in water. *J. Am. Chem. Soc.* **2003**, *125*, 9584−9585.

(17) (a) Qiu, Y.; Qin, Y.; Ma, Z.; Xia, W. Chitosan-supported zinc nitrate: preparation and catalyst for condensation reaction of aldehydes, amines, and terminal alkynes leading to the formation of propargylamines. *Chem. Lett.* **2014**, *43*, 1284−1286. (b) Eagalapati, N. P.; Rajack, A.; Murthy, Y. L. N. Nano-size ZnS: A novel, efficient and recyclable catalyst for A3-coupling reaction of propargylamines. *J. Mol. Catal. A: Chem.* **2014**, *381*, 126−131.

(18) Singh, D.; Singh, K. N. Highly efficient cadmium-catalyzed three-component coupling of an aldehyde, alkyne, and amine via CH Activation under microwave conditions. *Synlett* **2011**, 373−377.

(19) Pin-Hua, L.; Wang, L. Mercurous chloride catalyzed mannich condensation of terminal alkynes with secondary amines and aldehydes. *Chin. J. Chem.* **2005**, *23*, 1076−1080.

DOI: 10.1021/acsomega.9b01720
ACS Omega 2019, 4, 13991−14003

(20) Astruc, D. *Nanoparticles and Catalysis*; Wiley-VCH: Weinheim, 2008.
(21) Polshettiwar, V.; Varma, R. S. Green chemistry by nano-catalysis. *Green Chem.* **2010**, *12*, 743−754.
(22) (a) Deng, Y.; Li, E.; Cheng, X.; Zhu, J.; Lu, S.; Ge, C.; Gu, H.; Pan, Y. Facile preparation of hybrid core-shell nanorods for photothermal and radiation combined therapy. *Nanoscale* **2016**, *8*, 3895−3899. (b) Baran, T. Bio-synthesis and structural characterization of highly stable silver nanoparticles decorated on a sustainable bio-composite for catalytic reduction of nitroarenes. *J. Mol. Struct.* **2019**, *1182*, 213−218. (c) Baran, T. Biosynthesis of highly retrievable magnetic palladium nanoparticles stabilized on bio-composite for production of various biaryl compounds and catalytic reduction of 4-nitrophenol. *Catal. Lett.* **2019**, *149*, 1721−1729. (d) Baran, T. Production and application of highly efficient and reusable palladium nanocatalyst decorated on the magnetically retrievable chitosan/activated carbon composite microcapsules. *Catal. Lett.* **2019**, *149*, 1496−1503. (e) Baran, T. Pd(0) nanocatalyst stabilized on a novel agar/pectin composite and its catalytic activity in the synthesis of biphenyl compounds by Suzuki-Miyaura cross coupling reaction and reduction of o-nitroaniline. *Carbohydr. Polym.* **2018**, *195*, 45−52. (f) Baran, T.; Yılmaz Baran, N.; Menteş, A. An easily recoverable and highly reproducible agar-supported palladium catalyst for Suzuki-Miyaura coupling reactions and reduction of o-nitroaniline. *Int. J. Biol. Macromol.* **2018**, *115*, 249−256. (g) Baran, T. Ultrasound-accelerated synthesis of biphenyl compounds using novel Pd (0) nanoparticles immobilized on bio-composite. *Ultrason. Sonochem.* **2018**, *45*, 231−237. (h) Baran, N. Y.; Baran, T.; Menteş, A. Production of novel palladium nanocatalyst stabilized with sustainable chitosan/cellulose composite and its catalytic performance in Suzuki-Miyaura coupling reactions. *Carbohydr. Polym.* **2018**, *181*, 596−604. (j) Baran, T.; Yılmaz Baran, N.; Menteş, A. Sustainable chitosan/starch composite material for stabilization of palladium nanoparticles: Synthesis, characterization and investigation of catalytic behaviour of Pd@chitosan/starch nanocomposite in Suzuki−Miyaura reaction. *Appl. Organomet. Chem.* **2018**, *32*, No. e4075.
(23) Shokouhimehr, M.; Shin, K.-Y.; Lee, J. S.; Hackett, M. J.; Jun, S. W.; Oh, M. H.; Jang, J.; Hyeon, T. Magnetically recyclable core-shell nanocatalysts for efficient heterogeneous oxidation of alcohols. *J. Mater. Chem. A* **2014**, *2*, 7593−7599.
(24) Tsang, S. C.; Caps, V. R.; Paraskevas, I.; Chadwick, D.; Thompsett, D. Magnetically separable, carbon-supported nano-catalysts for the manufacture of fine chemicals. *Angew. Chem.* **2004**, *116*, 5763−5767.
(25) Shylesh, S.; Schünemann, V.; Thiel, W. R. Magnetically separable nanocatalysts: bridges between homogeneous and heterogeneous catalysis. *Angew. Chem., Int. Ed.* **2010**, *49*, 3428−3459.
(26) Gawande, M. B.; Branco, P. S.; Varma, R. S. Nano-magnetite (Fe_3O_4) as a support for recyclable catalysts in the development of sustainable methodologies. *Chem. Soc. Rev.* **2013**, *42*, 3371−3393.
(27) Zhang, D.; Zhou, C.; Sun, Z.; Wu, L.-Z.; Tung, C.-H.; Zhang, T. Magnetically recyclable nanocatalysts (MRNCs): a versatile integration of high catalytic activity and facile recovery. *Nanoscale* **2012**, *4*, 6244−6255.
(28) Wu, L.; Mendoza-Garcia, A.; Li, Q.; Sun, S. Organic phase syntheses of magnetic nanoparticles and their applications. *Chem. Rev.* **2016**, *116*, 10473−10512.
(29) Xuan, S.; Wang, Y.-X. J.; Yu, J. C.; Leung, K. C.-F. Preparation, characterization, and catalytic activity of core/shell Fe_3O_4@polyaniline@Au nanocomposites. *Langmuir* **2009**, *25*, 11835−11843.
(30) Guo, W.; Jiao, J.; Tian, K.; Tang, Y.; Jia, Y.; Li, R.; Xu, Z.; Wang, H. Controllable synthesis of core-satellite Fe_3O_4@polypyrrole/Pd nanoarchitectures with aggregation-free Pd nanocrystals confined into polypyrrole satellites as magnetically recoverable and highly efficient heterogeneous catalysts. *RSC Adv.* **2015**, *5*, 102210−102218.
(31) Chen, F.; Chen, A. A Facile one-pot Route to one-dimensional Fe_3O_4−polypyrrole nanocomposites. *Chem. Lett.* **2014**, *43*, 1809−1811.
(32) Xie, Y.; Yan, B.; Xu, H.; Chen, J.; Liu, Q.; Deng, Y.; Zeng, H. Highly regenerable mussel-inspired Fe_3O_4@polydopamine-Ag core−shell microspheres as catalyst and adsorbent for methylene blue removal. *ACS Appl. Mater. Interfaces* **2014**, *6*, 8845−8852.
(33) Zhai, Q.-G.; Hu, M.-C.; Li, S.-N.; Jiang, Y.-C. Synthesis, structure and blue luminescent properties of a new silver (I) triazolate coordination polymer with 8 2 10-a topology. *Inorg. Chim. Acta* **2009**, *362*, 1355−1357.
(34) Lee, D.; Cohen, R. E.; Rubner, M. F. Antibacterial properties of Ag nanoparticle loaded multilayers and formation of magnetically directed antibacterial microparticles. *Langmuir* **2005**, *21*, 9651−9659.
(35) Dai, Q.; Wei, T.; Lv, C.; Chai, F. Facile preparation of Ag nanoparticles using uric acid and their applications in colorimetric detection and catalysis. *Anal. Methods* **2018**, *10*, 4518−4524.
(36) Luo, X.; Morrin, A.; Killard, A. J.; Smyth, M. R. Application of nanoparticles in electrochemical sensors and biosensors. *Electroanalysis* **2006**, *18*, 319−326.
(37) Mitsudome, T.; Mikami, Y.; Funai, H.; Mizugaki, T.; Jitsukawa, K.; Kaneda, K. Oxidant-free alcohol dehydrogenation using a reusable hydrotalcite-supported silver nanoparticle catalyst. *Angew. Chem.* **2008**, *120*, 144−147.
(38) Guan, Y.; Li, Y.; van Santen, R. A.; Hensen, E. J. M.; Li, C. Controlling reaction pathways for alcohol dehydration and dehydrogenation over FeSBA-15 catalysts. *Catal. Lett.* **2007**, *117*, 18−24.
(39) Pradhan, N.; Pal, A.; Pal, T. Silver nanoparticle catalyzed reduction of aromatic nitro compounds. *Colloids Surf., A* **2002**, *196*, 247−257.
(40) Cong, H.; Becker, C. F.; Elliott, S. J.; Grinstaff, M. W.; Porco, J. A., Jr. Silver nanoparticle-catalyzed Diels-Alder cycloadditions of 2′-hydroxychalcones. *J. Am. Chem. Soc.* **2010**, *132*, 7514−7518.
(41) Narayanan, R.; El-Sayed, M. A. Catalysis with transition metal nanoparticles in colloidal solution: Nanoparticle shape dependence and stability. *J. Phys. Chem. B* **2005**, *109*, 12663−12676.
(42) Motokura, K.; Fujita, N.; Mori, K.; Mizugaki, T.; Ebitani, K.; Kaneda, K. One-pot synthesis of α-alkylated nitriles with carbonyl compounds through consecutive aldol reaction/hydrogenation using a hydrotalcite-supported palladium nanoparticle as a multifunctional heterogeneous catalyst. *Tetrahedron Lett.* **2005**, *46*, 5507−5510.
(43) Liu, C. H.; Zhou, Z. D.; Yu, X.; Lv, B. Q.; Mao, J. F.; Xiao, D. Preparation and characterization of Fe_3O_4/Ag composite magnetic nanoparticles. *Inorg. Mater.* **2008**, *44*, 291−295.
(44) Zhang, D.-H.; Li, G.-D.; Li, J.-X.; Chen, J.-S. One-pot synthesis of Ag−Fe_3O_4 nanocomposite: a magnetically recyclable and efficient catalyst for epoxidation of styrene. *Chem. Commun.* **2008**, 3414−3416.
(45) Zhu, S.; Fan, C.; Wang, J.; He, J.; Liang, E.; Chao, M. Realization of high sensitive SERS substrates with one-pot fabrication of Ag- Fe_3O_4 nanocomposites. *J. Colloid Interface Sci.* **2015**, *438*, 116−121.
(46) Chen, J.; Liu, Y.; Zhu, G.; Yuan, A. Ag@Fe_3O_4 nanowire: fabrication, characterization and peroxidase-like activity. *Cryst. Res. Technol.* **2014**, *49*, 309−314.
(47) Lopes, G.; Vargas, J. M.; Sharma, S. K.; Béron, F.; Pirota, K. R.; Knobel, M.; Rettori, C.; Zysler, R. D. Ag- Fe_3O_4 Dimer colloidal nanoparticles: Synthesis and enhancement of magnetic properties. *J. Phys. Chem. C* **2010**, *114*, 10148−10152.
(48) Li, S.; Zhou, Z.; Zhang, T.; Jiang, G.; Su, R. Synthesis and characterization of Ag/Fe_3O_4 electromagnetic shielding particles. *J. Magn. Magn. Mater.* **2014**, *358*−*359*, 27−31.
(49) Veisi, H.; Hemmati, S.; Javaheri, H. N-Arylation of indole and aniline by a green synthesized CuO nanoparticles mediated by Thymbra spicata leaves extract as a recyclable and heterogeneous nanocatalyst. *Tetrahedron Lett.* **2017**, *58*, 3155−3159.
(50) Ghaffari-Moghaddam, M.; Hadi-Dabanlou, R. Plant mediated green synthesis and antibacterial activity of silver nanoparticles using Crataegus douglasii fruit extract. *J. Ind. Eng. Chem.* **2014**, *20*, 739−744.

DOI: 10.1021/acsomega.9b01720
ACS Omega 2019, 4, 13991−14003

(51) Zargar, M.; Shameli, K.; Najafi, G. R.; Farahani, F. Plant mediated green biosynthesis of silver nanoparticles using Vitex negundo L. extract. *J. Ind. Eng. Chem.* **2014**, *20*, 4169−4175.
(52) Veisi, H.; Ghorbani-Vaghei, R.; Hemmati, S.; Aliani, M. H.; Ozturk, T. Green and effective route for the synthesis of monodispersed palladium nanoparticles using herbal tea extract (Stachys lavandulifolia) as reductant, stabilizer and capping agent, and their application as homogeneous and reusable catalyst in Suzuki coupling reactions in water. *Appl. Organomet. Chem.* **2015**, *29*, 26−32.
(53) Saravanakumar, A.; Ganesh, M.; Jayaprakash, J.; Jang, H. T. Biosynthesis of silver nanoparticles using Cassia tora leaf extract and its antioxidant and antibacterial activities. *J. Ind. Eng. Chem.* **2015**, *28*, 277−281.
(54) Anthony, K. J. P.; Murugan, M.; Jeyaraj, M.; Rathinam, N. K.; Sangiliyandi, G. Synthesis of silver nanoparticles using pine mushroom extract: A potential antimicrobial agent against E. coli and B. subtilis. *J. Ind. Eng. Chem.* **2014**, *20*, 2325−2331.
(55) Ramachandran, K.; Kalpana, D.; Sathishkumar, Y.; Lee, Y. S.; Ravichandran, K.; kumar, G. G. A facile green synthesis of silver nanoparticles using Piper betle biomass and its catalytic activity toward sensitive and selective nitrite detection. *J. Ind. Eng. Chem.* **2016**, *35*, 29−35.
(56) Ghahreman, A. *Basic Pharmacogenosy*; Tehran University Publication: Tehran, 2006; Vol. 3.
(57) Karimi, H. *A Dictionary of Iran's Vegetation Plants*; Parcham: Tehran, 2002.
(58) Zargary, A. *Medical Plants*; Tehran University Press: Tehran, 1990.
(59) Derksen, G. C. H.; van Beek, T. A.; de Groot, Æ.; Capelle, A. High-performance liquid chromatographic method for the analysis of anthraquinone glycosides and aglycones in madder root (Rubia tinctorum L.). *J. Chromatogr. A* **1998**, *816*, 277−281.
(60) El-Emary, N. A.; Backheet, E. Y. Three hydroxymethylanthraquinone glycosides from Rubia tinctorum. *Phytochemistry* **1998**, *49*, 277−279.
(61) Kawasaki, Y.; Goda, Y.; Yoshihira, K. The mutagenic constituents of Rubia tinctorum. *Chem. Pharm. Bull.* **1992**, *40*, 1504−1509.
(62) Marczylo, T.; Arimoto-Kobayashi, S.; Hayatsu, H. Protection against Trp-P-2 mutagenicity by purpurin: mechanism of in vitro antimutagenesis. *Mutagenesis* **2000**, *15*, 223−228.
(63) Schneider, H. J.; Unger, G.; Rössler, D.; Bothor, C.; Berg, W.; Ernst, G. Effect of drugs used for the prevention of urinary calculi recurrence on the growth and metabolism of young experimental animals. *Z. Urol. Nephrol.* **1979**, *72*, 237−247.
(64) Tundo, P.; Anastas, P.; Black, D. S.; Breen, J.; Collins, T. J.; Memoli, S.; Miyamoto, J.; Polyakoff, M.; Tumas, W. Synthetic pathways and processes in green chemistry. Introductory overview. *Pure Appl. Chem.* **2000**, *72*, 1207−1228.
(65) Schlögl, R. Heterogeneous catalysis. *Angew. Chem., Int. Ed.* **2015**, *54*, 3465−3520.
(66) (a) Veisi, H.; Taheri, S.; Hemmati, S. Preparation of polydopamine sulfamic acid-functionalized magnetic Fe_3O_4 nanoparticles with a core/shell nanostructure as heterogeneous and recyclable nanocatalysts for the acetylation of alcohols, phenols, amines and thiols under solvent-free conditions. *Green Chem.* **2016**, *18*, 6337−6348. (b) Bonyasi, F.; Hekmati, M.; Veisi, H. Preparation of core/shell nanostructure Fe_3O_4@PEG400-SO_3H as heterogeneous and magnetically recyclable nanocatalyst for one-pot synthesis of substituted pyrroles by Paal-Knorr reaction at room temperature. *J. Colloid Interface Sci.* **2017**, *496*, 177−187. (c) Pirhayati, M.; Veisi, H.; Kakanejadifard, A. Palladium stabilized by 3, 4-dihydroxypyridine-functionalized magnetic Fe_3 O_4 nanoparticles as a reusable and efficient heterogeneous catalyst for Suzuki reactions. *RSC Adv.* **2016**, *6*, 27252−27259. (d) Khakiani, B. A.; Pourshamsian, K.; Veisi, H. A highly stable and efficient magnetically recoverable and reusable Pd nanocatalyst in aqueous media heterogeneously catalysed Suzuki C−C cross-coupling reactions. *Appl. Organomet. Chem.* **2015**, *29*, 259−265. (e) Veisi, H.; Sedrpoushan, A.; Hemmati, S. Palladium supported on diaminoglyoxime-functionalized Fe_3O_4 nanoparticles as a magnetically separable nanocatalyst in Heck coupling reaction. *Appl. Organomet. Chem.* **2015**, *29*, 825−828. (f) Veisi, H.; Sedrpoushan, A.; Faraji, A. R.; Heidari, M.; Hemmati, S.; Fatahi, B. A mesoporous SBA-15 silica catalyst functionalized with phenylsulfonic acid groups (SBA-15-Ph-SO_3H) as a novel hydrophobic nanoreactor solid acid catalyst for a one-pot three-component synthesis of 2H-indazolo [2, 1-b] phthalazine-triones and triazolo [1, 2-a] indazole-triones. *RSC Adv.* **2015**, *5*, 70498. (g) Ghorbani-Vaghei, R.; Chegini, M.; Veisi, H.; Karimi-Tabar, M. Poly (N, N′-dibromo-N-ethyl-benzene-1, 3-disulfonamide), N, N, N′, N′-tetrabromobenzene-1, 3-disulfonamide and novel poly (N, N′-dibromo-N-phenylbenzene-1, 3-disulfonamide) as powerful reagents for benzylic bromination. *Tetrahedron Lett.* **2009**, *50*, 1861−1865. (h) Veisi, H.; Hemmati, S.; Qomi, M. Aerobic oxidation of benzyl alcohols through biosynthesized palladium nanoparticles mediated by Oak fruit bark extract as an efficient heterogeneous nanocatalyst. *Tetrahedron Lett.* **2017**, *58*, 4191−4196.
(67) Aromal, S. A.; Vidhu, V. K.; Philip, D. Green synthesis of well-dispersed gold nanoparticles using Macrotyloma uniflorum. *Spectrochim. Acta, Part A* **2012**, *85*, 99−104.
(68) (a) Veisi, H.; Faraji, A. R.; Hemmati, S.; Gil, A. Green synthesis of palladium nanoparticles using Pistacia atlantica kurdica gum and their catalytic performance in Mizoroki−Heck and Suzuki−Miyaura coupling reactions in aqueous solutions. *Appl. Organomet. Chem.* **2015**, *29*, 517−523. (b) Veisi, H.; Rashtiani, A.; Barjasteh, V. Biosynthesis of palladium nanoparticles using Rosa canina fruit extract and their use as a heterogeneous and recyclable catalyst for Suzuki−Miyaura coupling reactions in water. *Appl. Organomet. Chem.* **2016**, *30*, 231−235.
(69) Sheny, D. S.; Mathew, J.; Philip, D. Phytosynthesis of Au, Ag and Au−Ag bimetallic nanoparticles using aqueous extract and dried leaf of Anacardium occidentale. *Spectrochim. Acta, Part A* **2011**, *79*, 254−262.
(70) Nimse, S. B.; Pal, D. Free radicals, natural antioxidants, and their reaction mechanisms. *RSC Adv.* **2015**, *5*, 27986−28006.
(71) Kumar, V. A.; Uchida, T.; Mizuki, T.; Nakajima, Y.; Katsube, Y.; Hanajiri, T.; Maekawa, T. Synthesis of nanoparticles composed of silver and silver chloride for a plasmonic photocatalyst using an extract from a weed Solidago altissima (goldenrod). *Adv. Nat. Sci.: Nanosci. Nanotechnol.* **2016**, *7*, 015002−015014.
(72) Wang, W.; Tang, B.; Ju, B.; Gao, Z.; Xiu, J.; Zhang, S. Fe_3O_4-functionalized graphene nanosheet embedded phase change material composites: efficient magnetic-and sunlight-driven energy conversion and storage. *J. Mater. Chem. A* **2017**, *5*, 958−968.
(73) Bhuvaneswari, S.; Pratheeksha, P. M.; Anandan, S.; Rangappa, D.; Gopalan, R.; Rao, T. N. Efficient reduced graphene oxide grafted porous Fe_3O_4 composite as a high performance anode material for Li-ion batteries. *Phys. Chem. Chem. Phys.* **2014**, *16*, 5284−5294.
(74) Zhang, W.; Kong, C.; Lu, G. Super-paramagnetic nano-Fe_3O_4/graphene for visible-light-driven hydrogen evolution. *Chem. Commun.* **2015**, *51*, 10158−10161.
(75) Xiong, X.; Chen, H.; Zhu, R. Oyster shell waste supported $CuCl_2$ for aldehyde-alkyne-amine coupling reaction to propargylamines. *Chin. J. Catal.* **2014**, *35*, 2006−2013.
(76) Wei, C.; Li, Z.; Li, C.-J. The first silver-catalyzed three-component coupling of aldehyde, alkyne, and amine. *Org. Lett.* **2003**, *5*, 4473−4475.
(77) Karimi, B.; Gholinejad, M.; Khorasani, M. Highly efficient three-component coupling reaction catalyzed by gold nanoparticles supported on periodic mesoporous organosilica with ionic liquid framework. *Chem. Commun.* **2012**, *48*, 8961−8963.
(78) Zohreh, N.; Hosseini, S. H.; Jahani, M.; Xaba, M. S.; Meijboom, R. Stabilization of Au NPs on symmetrical tridentate NNN-Pincer ligand grafted on magnetic support as water dispersible and recyclable catalyst for coupling reaction of terminal alkyne. *J. Catal.* **2017**, *356*, 255−268.
(79) Cammarata, J. R.; Rivera, R.; Fuentes, F.; Otero, Y.; Ocando-Mavárez, E.; Arce, A.; Garcia, J. M. Single and double A^3-coupling

DOI: 10.1021/acsomega.9b01720
ACS Omega 2019, 4, 13991−14003

(aldehyde-amine-alkyne) reaction catalyzed by an air stable copper (I)-phosphole complex. *Tetrahedron Lett.* **2017**, *58*, 4078−4081.
(80) Yadav, J. S.; Subba Reddy, B. V.; Hara Gopal, A. V.; Patil, K. S. $InBr_3$-catalyzed three-component reaction: a facile synthesis of propargyl amines. *Tetrahedron Lett.* **2009**, *50*, 3493−3496.
(81) Yan, W.; Wang, R.; Xu, Z.; Xu, J.; Lin, L.; Shen, Z.; Zhou, Y. A novel, practical and green synthesis of Ag nanoparticles catalyst and its application in three-component coupling of aldehyde, alkyne, and amine. *J. Mol. Catal. A: Chem.* **2006**, *255*, 81−85.
(82) Maggi, R.; Bello, A.; Oro, C.; Sartori, G.; Soldi, L. AgY zeolite as catalyst for the effective three-component synthesis of propargylamines. *Tetrahedron* **2008**, *64*, 1435−1439.
(83) Movahedi, F.; Masrouri, H.; Kassaee, M. Z. Immobilized silver on surface-modified ZnO nanoparticles: As an efficient catalyst for synthesis of propargylamines in water. *J. Mol. Catal. A: Chem.* **2014**, *395*, 52−57.
(84) Li, P.; Wang, L.; Zhang, Y.; Wang, M. Highly efficient three-component (aldehyde−alkyne−amine) coupling reactions catalyzed by a reusable PS-supported NHC−Ag(I) under solvent-free reaction conditions. *Tetrahedron Lett.* **2008**, *49*, 6650−6654.
(85) Patel, S. B.; Vasava, D. V. Carbon nitride-supported silver nanoparticles: Microwave-assisted synthesis of propargylamine and oxidative C-C coupling reaction. *ChemistrySelect* **2018**, *3*, 471−480.
(86) Veisi, H.; Kazemi, S.; Mohammadi, P.; Safarimehr, P.; Hemmati, S. Catalytic reduction of 4-nitrophenol over Ag nanoparticles immobilized on Stachys lavandulifolia extract-modified multi walled carbon nanotubes. *Polyhedron* **2019**, *157*, 232−240.

DOI: 10.1021/acsomega.9b01720
ACS Omega 2019, 4, 13991−14003